Supplementary Information (SI) for Nanoscale Horizons.
This journal is © The Royal Society of Chemistry 2024

Supporting Information

Low-resistivity Ohmic contacts of Ti/Al on few-layered 1T'-$MoTe_2$/2H-$MoTe_2$ heterojunction grown by chemical vapor deposition

Ping-Feng Chi [a], Jing-Jie Wang [b], Jing-Wen Zhang [b], Yung-Lan Chuang [a], Ming-Lun Lee[c,*], Jinn-Kong Sheu[a,b,*]

[a] Department of Photonics, National Cheng Kung University, Tainan City, Taiwan-70101.

[b] Academy of Innovative Semiconductor and Sustainable Manufacturing, National Cheng Kung University, Tainan City, Taiwan-70101.

[a] Department of Electro-Optical Engineering, Southern Taiwan University of Science and Technology, Tainan City, Taiwan-71001.

*Jinn-Kong Sheu, Email: jksheu@ncku.edu.tw

*Ming-Lun Lee, Email:minglun@stust.edu.tw

Fig. S1 shows a schematic diagram of the CW-CVD system used in this experiment. The SiC susceptor used in this system can accommodate up to 4-inch sapphire substrates (Al_2O_3 or SiO_2/Si substrates).

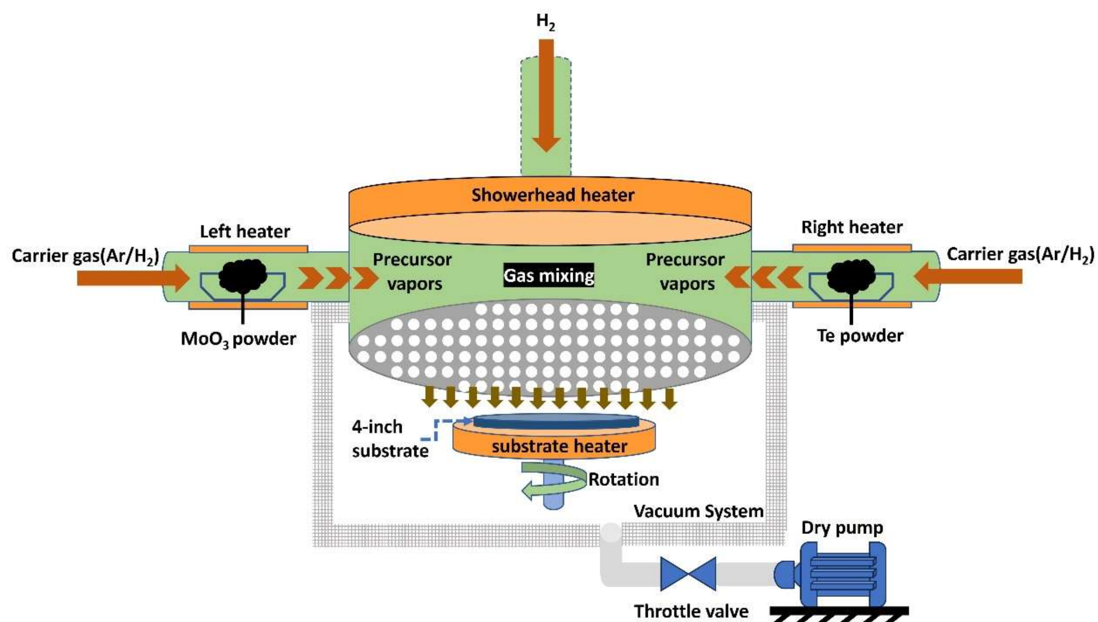

Fig. S1 Schematic diagram of a typical CWCVD synthesis system.

A typical growth process of the few-layered $MoTe_2$ thin films is described as follows:
1. The susceptor heater is heated to 700 °C, and the substrate is subjected to desorption treatment under a 75 torr H_2 environment to remove impurities and moisture from the substrate.
2. The susceptor heater is then adjusted to a temperature range of 650 to 700 °C, and the left heater is raised to 630 °C to vaporize the MoO_3 powder placed in the boat.
3. Argon (Ar) gas is introduced to carry the vaporized MoO_3 (precursor vapors) into the Gas Mixing Chamber under the showerhead. Simultaneously, H_2 reactive gas is introduced from above the showerhead, with an H_2/Ar ratio of 4:6. This process continues until the chamber pressure reaches 200 to 300 torr.
4. The mixture of gases is directed through the showerhead towards the substrate, where a nucleation layer begins to form.
5. The throttle valve angle is adjusted to reduce the pressure to 150 to 200 torr, and lateral growth of MoO_x continuous thin film occurs on the sapphire substrate.
6. The susceptor heater temperature is then decreased to a range of 400 to 500 °C, and the right heater is raised to 550 °C to vaporize the Te powder placed in the boat.
7. Similar to the MoO_3 vaporization process, Ar gas carries Te vapor (precursor vapors) into the Gas Mixing Chamber, and H_2 reactive gas is introduced with an H_2/Ar ratio of 2:8. The chamber pressure is increased to 500 torr.
8. In this Te-rich environment, the previously deposited MoO_x thin film is reacted with Te for 2 hours, transforming MoO_x into $MoTe_2$ thin film.

During the high growth rate process of MoO_x, the vaporization temperature of MoO_3 is increased to enhance the vapor amount of MoO_3, which then reacts with H_2. The large volume of MoO_3 vapor does not fully react with H_2, leading to the formation of suboxides MoO_{3-x} within the MoOx film. These suboxides are unable to bond with Te, resulting in a significant number of Te vacancies in $MoTe_2$, which in turn leads to the formation of the 1T' phase. The literature [1] suggests that Te vacancies cause $MoTe_2$ to transition to the 1T' phase. Fig. S2 shows the XPS analysis of the binding energy differences between high growth rate (H.G.R.)and low growth rate (L.G.R.) MoO_x.

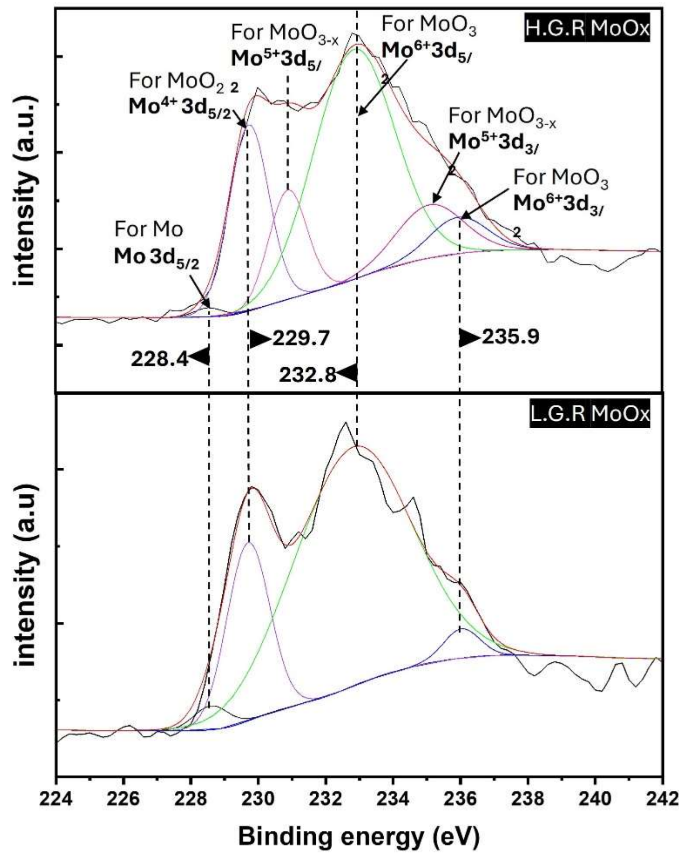

Fig. S2 compares the typical XPS spectra of Mo3$d_{5/2}$ and Mo3$d_{3/2}$ chemical binding energies between H.G.R. MoO_x and L.G.R. MoO_x.

Fig. S3 illustrates the growth temperature and pressure profiles for the epitaxial growth of few-layered 1T'-$MoTe_2$, 2H-$MoTe_2$, and vertically stacked 1T'/2H-$MoTe_2$ heterostructures.

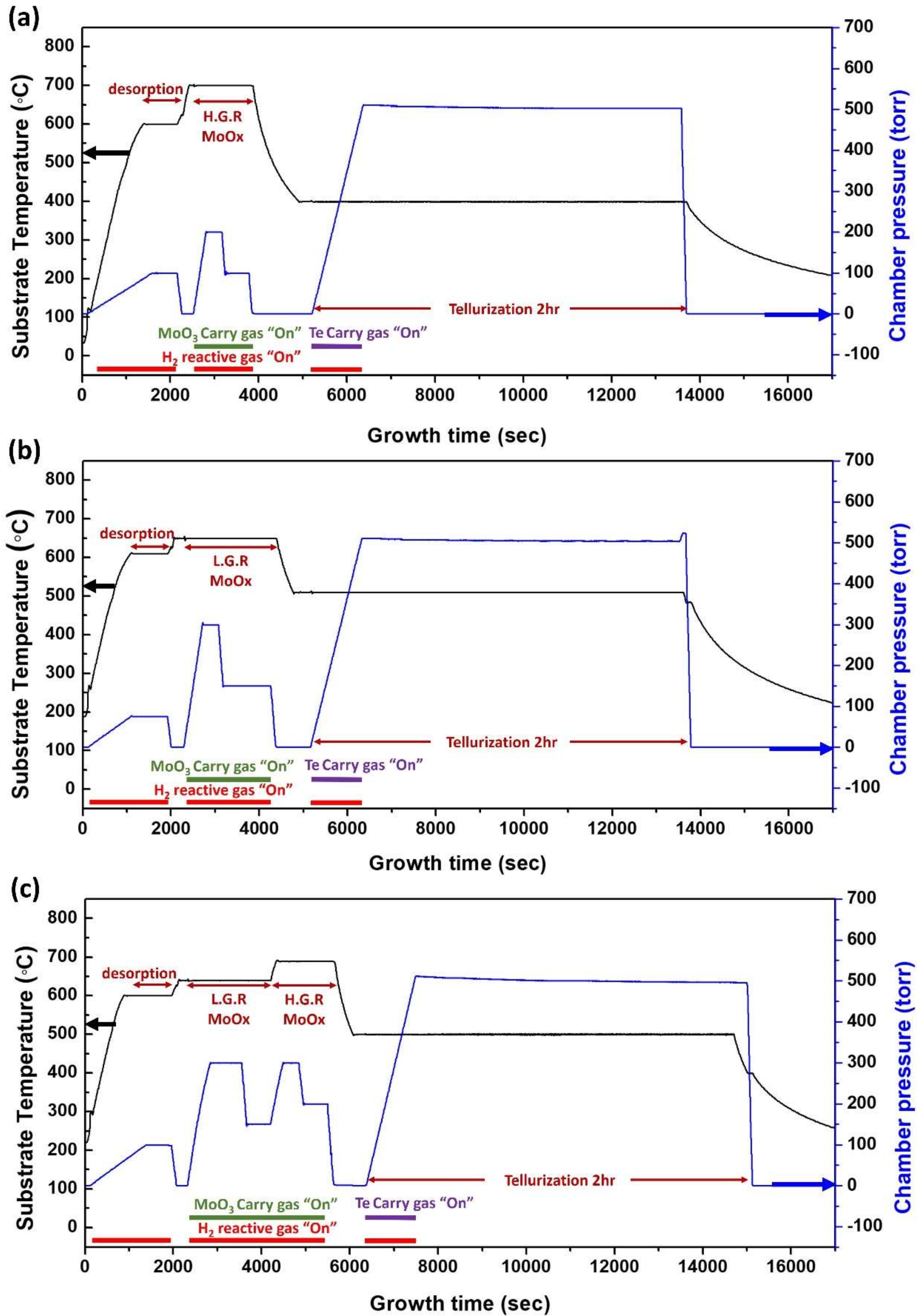

Fig. S3 Temperature and pressure profiles during the growth of $MoTe_2$ for (a) few-layered 1T'-$MoTe_2$ and (b) few-layered 2H-$MoTe_2$ (c) vertically stacked 2H/1T'-$MoTe_2$ heterostructure.

Fig. S4 shows the typical inspection of the $MoTe_2$ continuous thin films by cross-section High-Resolution Transmission Electron Microscopy (HR-TEM) performed on the wafers B, C, and D to determine the thicknesses of the few-layered $MoTe_2$ thin films grown on sapphire substrates. The typical thicknesses of the few-layered 2H-$MoTe_2$、1T'-$MoTe_2$, and 2H/1T'-$MoTe_2$ thin films were 3.1、2.3, and 7.6 nm, respectively. These thicknesses correspond to approximately 4, 3, and 10 layers.

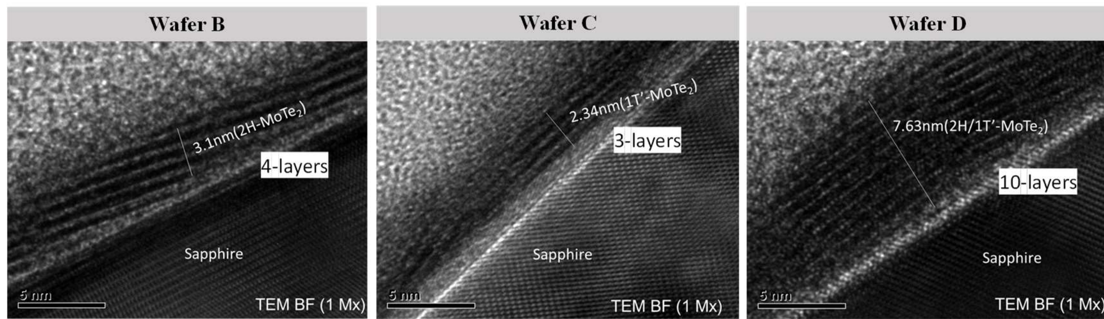

Fig. S3 shows the typical inspection of cross-section HR-TEM performed on wafers B, C, and D.

Figure S5 presents Raman spectra of few-layer 1T'-$MoTe_2$ and 2H-$MoTe_2$, measured at five locations on a 2-inch wafer. This indicates that the large-area and continuous $MoTe_2$ thin films on sapphire substrates have uniform thickness and stoichiometry.

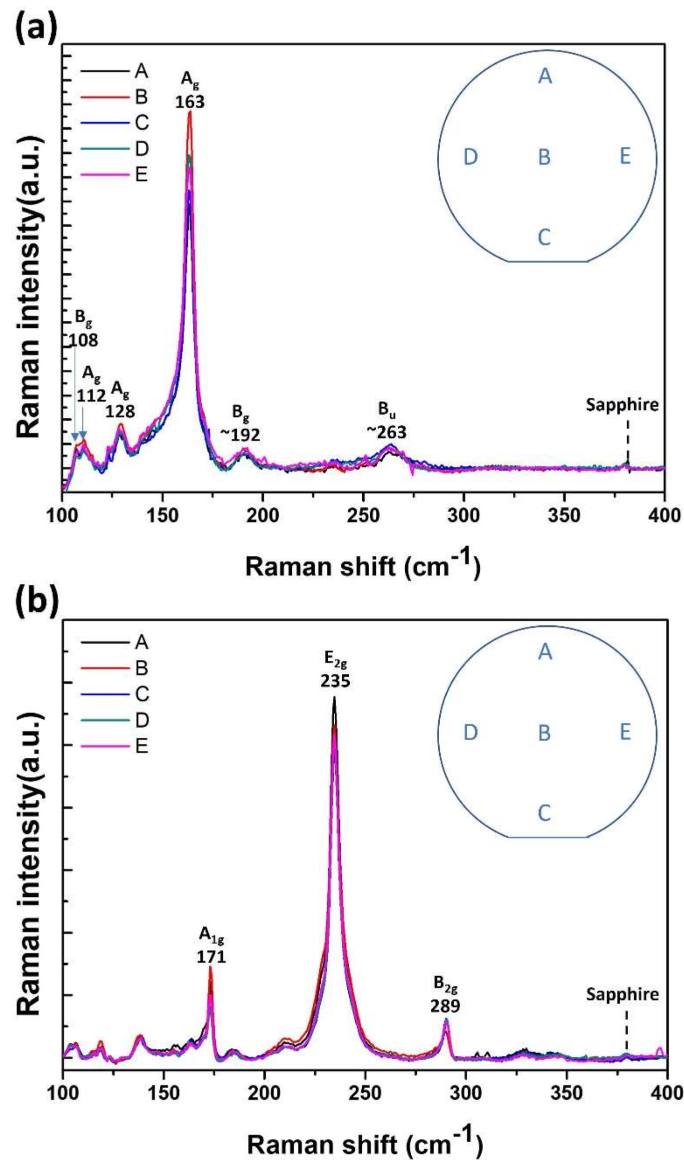

Fig. S5 Raman spectra were collected at five different points on a 2-inch wafer. The spectra for both few-layered 1T'-$MoTe_2$ and 2H-$MoTe_2$ are shown in (a) and (b), respectively.

Fig. S6 displays the intensity-normalized Raman spectra of 2H-/1T'-$MoTe_2$ heterostructures etched at different times. The intensities of characteristic peaks of the 1T'-$MoTe_2$ phase decreased with an increase in etching times, and they disappeared eventually. The Raman spectra confirm that the 1T'-$MoTe_2$ layers stack on the 2H-$MoTe_2$ layers.

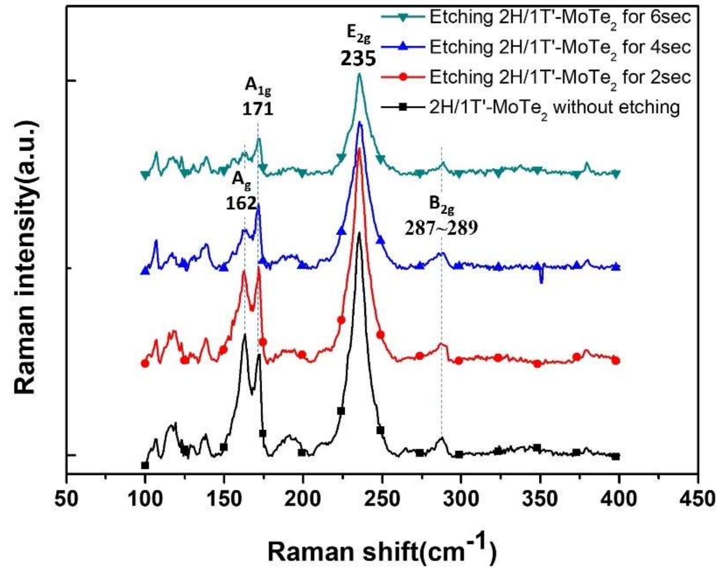

Fig. S6 Typical Raman spectra of the 2H/1T'-$MoTe_2$ structure at different etching times.

The process flow for the TLM contact patterns on both few-layered 2H-$MoTe_2$ and 2H/1T'-$MoTe_2$ stacked heterostructures is shown in Fig. S7.

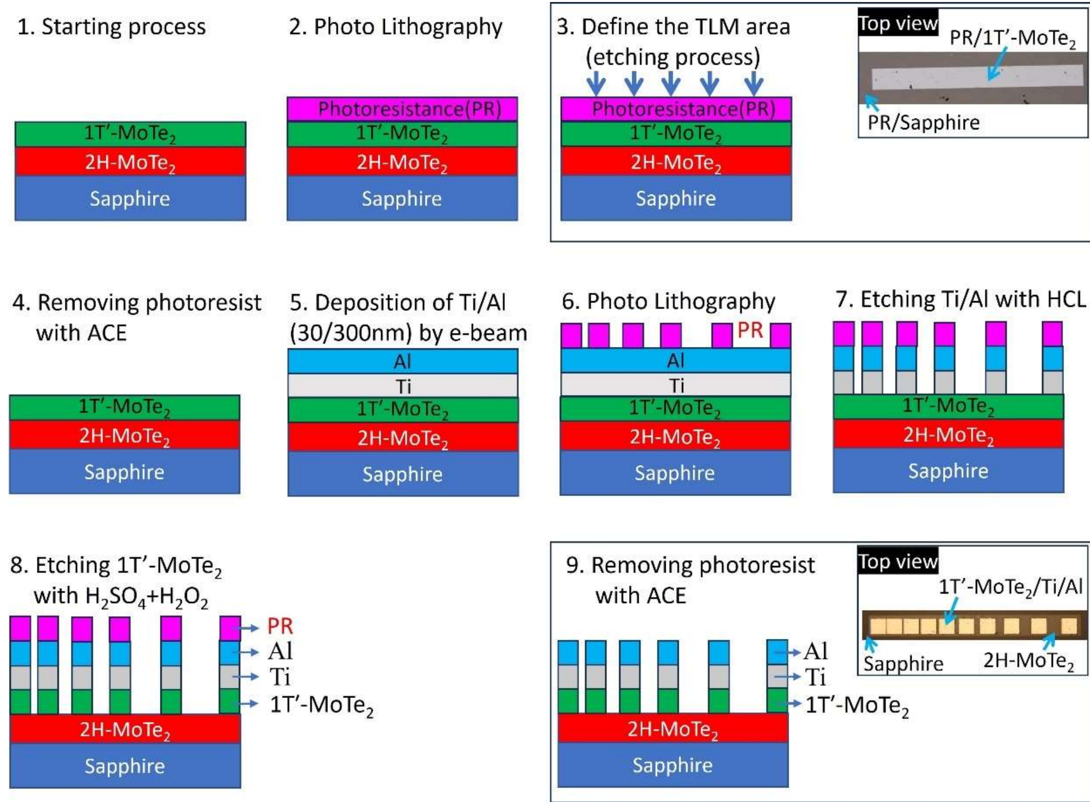

Fig. S7 Process flow for the TLM contact patterns on both few-layered 2H-$MoTe_2$ and 2H/1T'-$MoTe_2$ stacked heterostructures.

We observed the surface morphology of 2H-$MoTe_2$ and 1T'-$MoTe_2$ using AFM. Fig. S8 displays the surface morphology of the few-layer (a) 2H-$MoTe_2$ and (b) 1T'-$MoTe_2$. The results show that the root mean square (Rq) values for 2H-$MoTe_2$ and 1T'-$MoTe_2$ are 0.26 nm and 0.93 nm, respectively. The significantly higher Rq for 1T'-$MoTe_2$ suggests a rougher surface, potentially due to the oxidation of Te atoms. To confirm this hypothesis, we employed X-ray photoelectron spectroscopy (XPS) to analyze the elemental distribution and chemical composition of both materials. As expected, 1T'-$MoTe_2$ exhibits binding energies consistent with TeO_2 [2], indicating a higher propensity for oxygen adsorption and TeO_2 formation. Additionally, we quantified the Te content by integrating the Mo 3d and Te 3d peak areas from the XPS spectra [Figs. S9(a) and S9(b) for 2H-$MoTe_2$ and 1T'-$MoTe_2$, respectively] and applying atomic sensitivity factors. The calculated Te atomic ratios for 2H-$MoTe_2$ and 1T'-$MoTe_2$ are 1.96 and 1.53, respectively. Ideally, each Mo atom should bond with two Te atoms, resulting in a Te:Mo ratio of 2. A ratio lower than 2 signifies an increase in Te vacancies.

Therefore, the lower Te:Mo ratio in 1T'-$MoTe_2$ suggests a higher concentration of Te vacancies, which aligns with the findings by Kim, H. et al.[1].

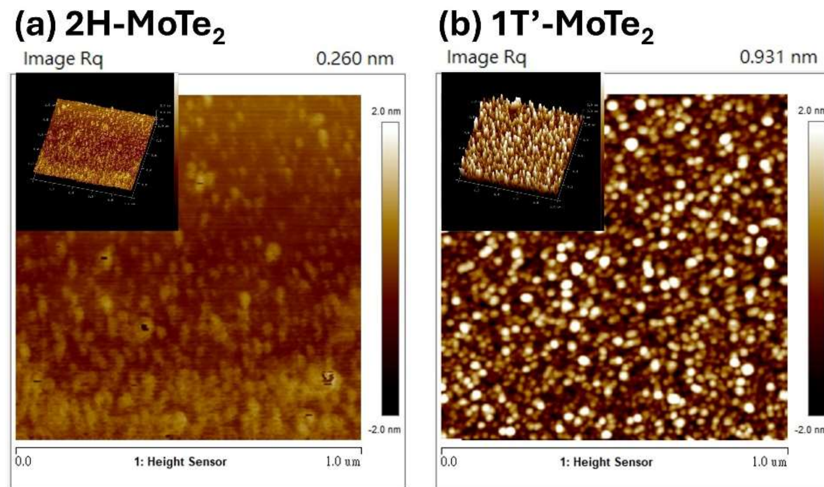

Fig. S8 Typical surface morphology of (a) 2H-$MoTe_2$ and (b) 1T'-$MoTe_2$ observed through AFM.

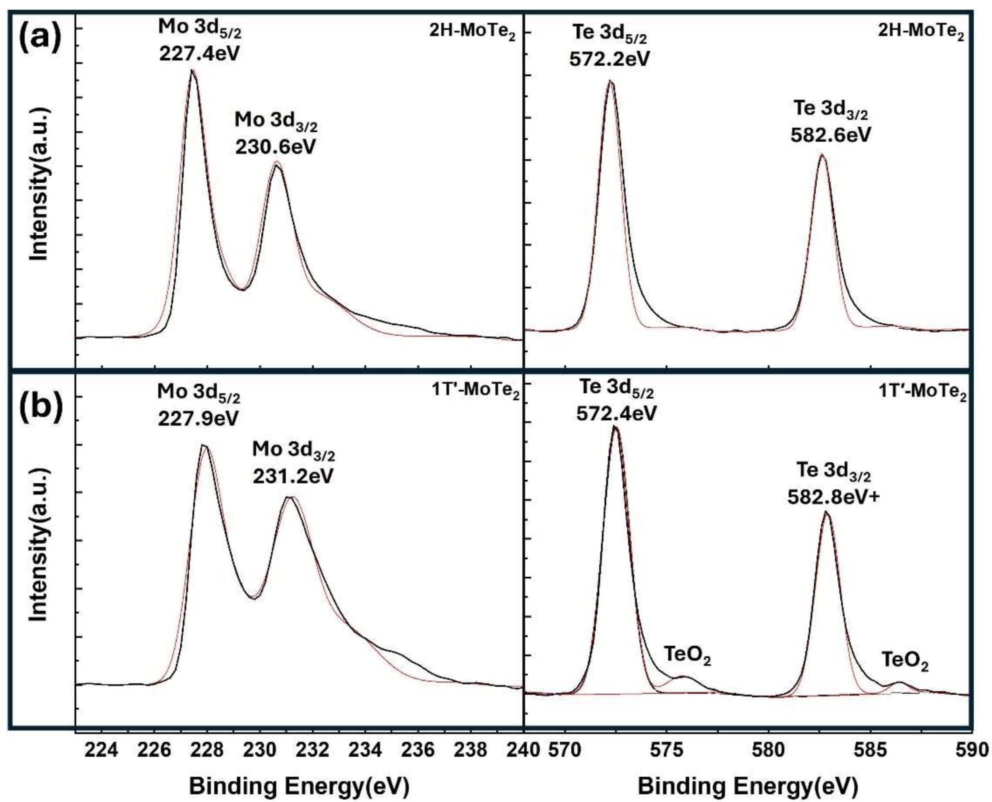

Fig. S9 Typical chemical bonding energies of Te and Mo in the few-layer (a) 2H-$MoTe_2$ and (b) 1T'-$MoTe_2$ analyzed by XPS.

The CW-CVD reactor, as shown in Fig.S1, was also used to grow the few-layer $MoTe_2$ films on both SiO_2/Si and Al_2O_3/Si substrates. However, initial results showed a slightly wavy interface between the $MoTe_2$ film and the Al_2O_3 template layer ((Fig. S10(b)), unlike the flat interface observed for the few-layer 2H-$MoTe_2$ grown on the sapphire substrate ((Fig. S10(a)).

Raman spectroscopy further indicated that the few-layer 2H-$MoTe_2$ grown on sapphire exhibited superior film quality, as shown in Fig. S11. This difference can be attributed to the surface roughness of the Al_2O_3 template layer. Additionally, In our previous lab work, we attempted to use SiO_2/Si substrates with a PECVD-deposited SiO_2 template layer for the growth of the few-layer 2H-$MoTe_2$. However, TEM results revealed a wavy interface for few-layer $MoTe_2$ on the SiO_2 /Si substrate, and AFM analyses confirmed that the wavy interface was caused by the inferior flatness of the SiO_2 layer, as shown in Fig. S12. These findings informed our choice of single-crystal Al_2O_3 as the growth substrates in this study.

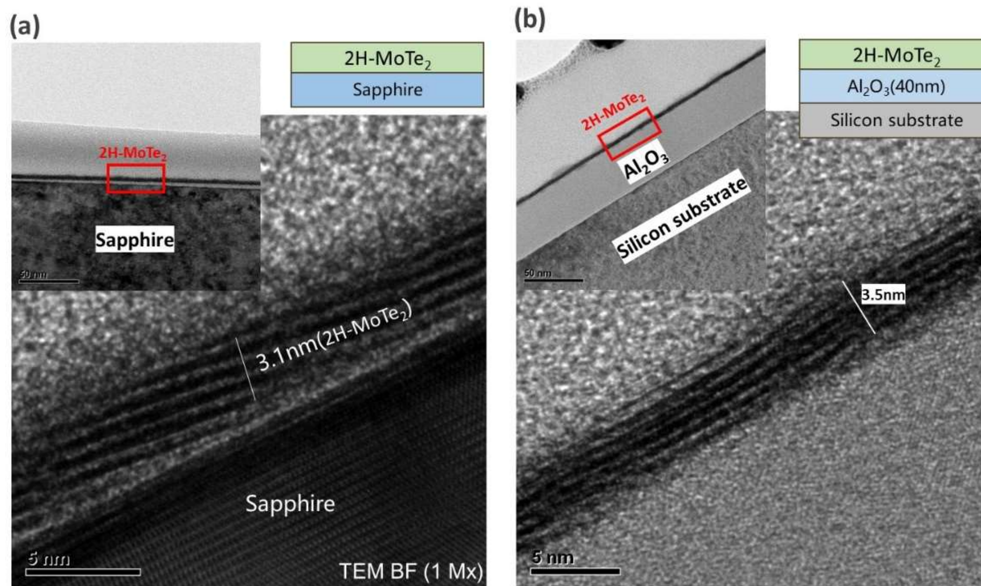

Fig. S10 Typical TEM images of 2H-$MoTe_2$ grown on (a) a sapphire substrate and (b) a Si substrate/Al_2O_3.

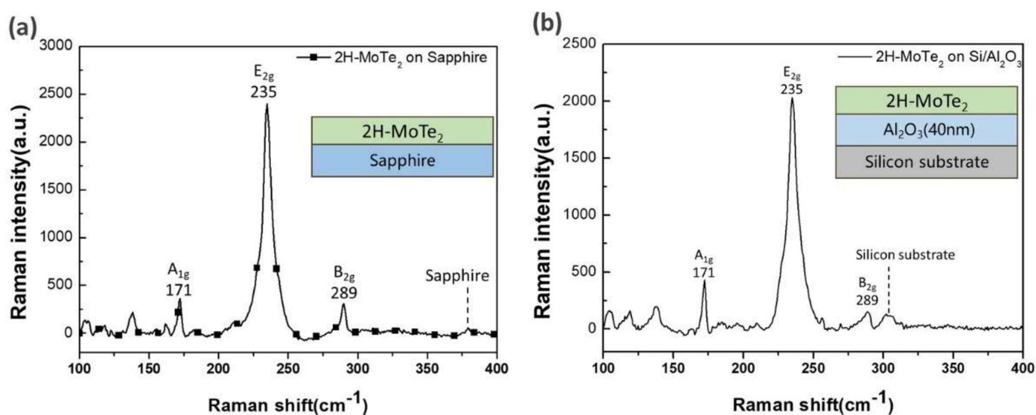

Fig. S11 Raman spectra of 2H-$MoTe_2$ grown on (a) a sapphire substrate and (b) a Si substrate/Al_2O_3.

While deposited using PECVD and e-beam evaporation, respectively, both the surface amorphous SiO_2 and Al_2O_3 layers on the Si substrate remained too rough for the growth of high-quality few-layer 2H-$MoTe_2$. AFM measurements confirmed that the surface roughness of these template layers exceeded that of the sapphire substrate.
Our findings suggest that template layers like SiO_2 and Al_2O_3 require sub-nanometer surface roughness to achieve high-quality growth of a few-layer 2H-$MoTe_2$.

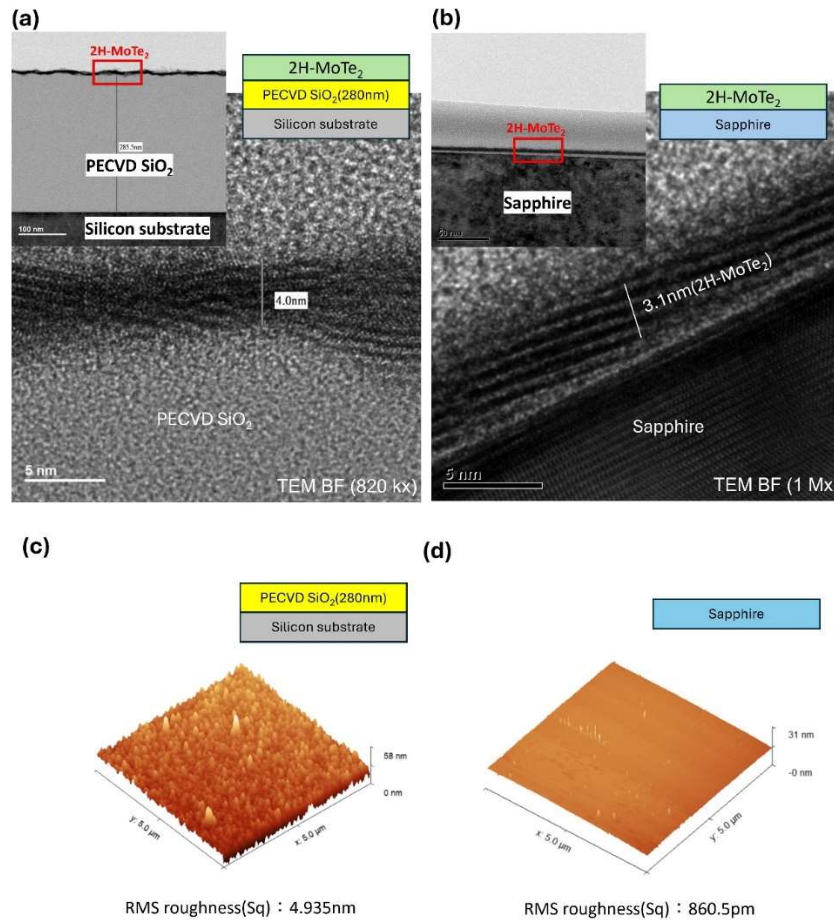

Fig. S12 Typical cross-section TEM images taken from the few-layer 2H-$MoTe_2$ grown on (a) SiO_2/Si substrate and (b) Sapphire. The insets depict the schematic layer structures. Typical AFM images were taken from the surface of (c) SiO_2/Si and (d) sapphire substrates to determine the surface roughness.

References

1 Kim, H. *et al.* Elucidating atomistic mechanisms of the formation of phase-controlled ultrathin $MoTe_2$ films and lateral hetero-phase $MoTe_2$ interfaces. *Surfaces and Interfaces* **40**, 103040 (2023).

2. Wu, D. *et al.* Phase-controlled van der Waals growth of wafer-scale 2D $MoTe_2$ layers for integrated high-sensitivity broadband infrared photodetection. *Light: Science & Applications* **12**, 5 (2023).